

The role of surface elasticity in liquid film formation: unifying Frankel and Landau-Levich-Derjaguin configurations.

Lorène Champougny,¹ Benoit Scheid,^{2, a)} Frédéric Restagno,¹ and Emmanuelle Rio^{1, b)}

¹⁾*Laboratoire de Physique des Solides, CNRS & Université Paris-Sud, 91405 Orsay cedex, France*

²⁾*TIPs - Fluid Physics unit, Université Libre de Bruxelles C.P. 165/67, 1050 Brussels, Belgium*

The behavior of thin liquid films during their generation from a surfactant solution is investigated through comparison between a hydrodynamic model including surface elasticity and experiments. “Twin” models are proposed to describe the coating of films onto a solid plate (Landau-Levich-Derjaguin configuration) as well as soap film pulling (Frankel configuration). Experimental data from the literature are successfully fitted using the models, surface elasticity being the only adjustable parameter. For a given surfactant solution, the analyses of soap and coated films both yield the same value for surface elasticity. Conversely, this shows that Frankel- or Landau-Levich-like experiments can be used in practice as surface rheometers to determine the numerical value of the surface elasticity of a solution, especially for values lower than those measurable by classical devices.

I. INTRODUCTION

The formation of thin liquid films, either free standing (soap films) or deposited on a solid substrate (coated films), is of utmost importance for many applications. The thickness of soap films within a foam is indeed one of the key ingredients controlling foam destabilization through coalescence (rupture of a film separating two bubbles) and drainage (liquid flow through the Plateau border network). Understanding the physical and physicochemical parameters that control film thickness is thus necessary when stable foams are required, as in cosmetics or food products for instance, but also if quick foam collapse is sought for, as in washmachines¹. Additionally, the coating of thin liquid films onto solid substrates is a widespread industrial process, used for surface functionalization as well as surface protection or lubrication². In many cases, the deposition of a liquid layer of controlled thickness is needed. Understanding the influence of physicochemistry on film thickness is all the more crucial that complex liquids, such as colloidal dispersions or emulsions, are often used as coating agents³.

The major difference between free and coated films is that pure liquid films can be coated onto a solid substrate by viscous entrainment, whereas viscous forces alone are not sufficient to generate a free standing film^{4,5}. The additional support that helps pulling the soap film upwards stems from interfacial shear, which usually results from gradients in the concentration of surface active agents (surfactants) adsorbed at the liquid/air interfaces^{6,7}, but can also be generated by temperature gradients^{8,9}.

Despite their different fields of applications, the generation of a free standing film and the coating of a liquid film on a plate are very similar from the hydrodynamic point of view but have mostly been

^{a)}E-mail adress: bscheid@ulb.ac.be

^{b)}E-mail adress: emmanuelle.rio@u-psud.fr

studied separately in the literature. In particular, no quantitative parallel has been drawn, to our knowledge, between free films and coated films generated from identical surfactant solutions. The first hydrodynamic descriptions of those processes were respectively given by Frankel and Mysels⁶ for soap films and by Landau, Levich and Derjaguin¹⁰ for coated films. Both models are based on the same governing equations and yield the same scaling law for the thickness h_0 of a film pulled out of a liquid (density ρ , viscosity η , surface tension γ_0) at a constant velocity V :

$$h_0 = K \ell_c \text{Ca}^{2/3}, \quad (1)$$

where $\ell_c = \sqrt{\gamma_0/\rho g}$ is the capillary length (below which capillary effects are dominant over gravity g), $\text{Ca} = \eta V/\gamma_0$ is the capillary number and K is a numerical prefactor. This scaling law simply results from a balance between viscous entrainment and capillary suction and should be valid as long as $\text{Ca}^{1/3} \ll 1$. The value of the prefactor K in eq. (1) is obtained by asymptotically matching the curvatures of the static and dynamic meniscii and essentially depends on the film boundary conditions at the liquid/air interface. In the Landau-Levich-Derjaguin (LLD) configuration with a *pure* liquid, a no slip condition is taken at the solid/liquid interface while the liquid/air interface is simply assumed to be stress free; such boundary condition is here referred to as “fluid”. The predicted value¹⁰ for the prefactor in eq. (1) is

$$K_{\text{LLD}}^{\text{fluid}} = 0.9458, \quad (2)$$

which is in good agreement with experimental data^{11,12}. However, when pulling a free standing film out of a solution containing surface active agents, the presence of sustaining interfacial stresses must be accounted for in the boundary condition at the liquid/air interfaces¹³. This is the reason why, in their original work, Frankel and Mysels assumed that the interfaces behave as if entrained without slip by a solid wall; such boundary condition is here referred to as “rigid”. As a consequence of this choice of boundary conditions, Frankel’s model boils down to the LLD model with a factor 2, the liquid/air interfaces being viewed as two solid walls and the stress along the vertical symmetry axis of the free film being zero. In our notations (see figure 1), the prefactor in eq. (1) is still $K_{\text{LLD}}^{\text{fluid}} = K_{\text{Fr}}$ but the actual thickness of the soap film is twice the thickness of a pure liquid LLD film. In the LLD geometry, this limiting case of a rigid liquid/air interface changes the prefactor in eq. (1) into

$$K_{\text{LLD}}^{\text{rigid}} = 4^{2/3} K_{\text{LLD}}^{\text{fluid}}. \quad (3)$$

Note that $K_{\text{LLD}}^{\text{rigid}}$ is larger than $2K_{\text{Fr}}$, since the capillary suction that opposes the entrainment is caused by the presence of only one meniscus in the LLD case but two meniscii in the Frankel case.

This hydrodynamic hypothesis of rigid liquid/air interfaces was found in good qualitative agreement with many experiments for both Frankel^{7,14–18} and LLD^{11,19,20} configurations at low capillary numbers ($\text{Ca} < 10^{-5}$). It turned out to hold as well in other geometries, like fluid coating on fibers^{21,22} or bubbles moving in tubes²³. Nevertheless, the dispersion of data points was observed to be quite large from one experiment to another²⁴. Moreover, the film was found to be significantly thinner than predicted by eq. (1) at higher capillary numbers ($\text{Ca} \sim 10^{-5} - 10^{-4}$), although the condition $\text{Ca}^{1/3} \ll 1$ for neglecting gravitational drainage still holds^{12,14,18,25}.

Since the works by Frankel and Mysels on the one hand, and by Landau, Levich and Derjaguin on the other hand, many models^{5,26–31} have been proposed to refine the assumption of rigid interfaces in order to account for the dynamics of surfactants at the liquid/air interfaces. Most of the models make the assumption of water-insoluble surfactants, for which the interfacial dynamics and its description in terms of surface rheological properties³² is much simpler than for water-soluble

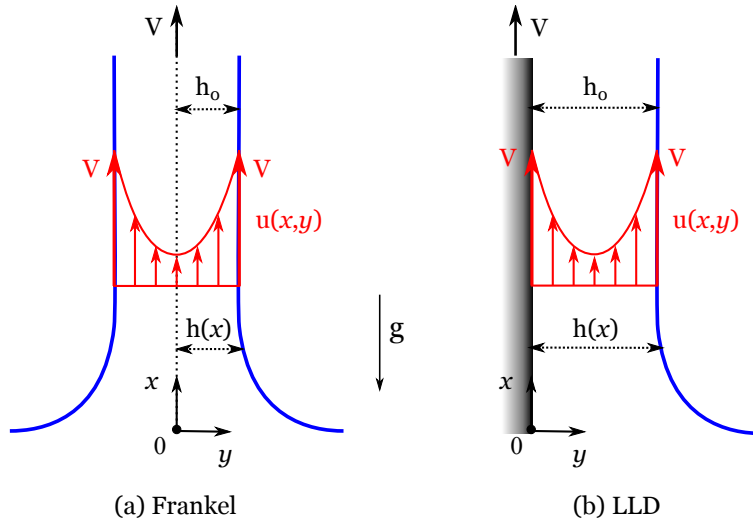


FIG. 1. Sketches introducing the main notations used in this paper for (a) Frankel configuration (soap film pulling) and (b) LLD configuration (plate coating). The vertical velocity field $u(x,y)$ is defined in the reference frame of the laboratory and is represented here in the case of rigid liquid/air interfaces in both Frankel and LLD configurations. Note that $h(x)$ is defined as half the film thickness for a soap film, whereas it stands for the actual thickness of a coated film.

surfactants. Quantitative comparison between those models and experimental data available on thin films formed from water-soluble surfactant solutions is thus to be done cautiously, but remains possible³³ if the surface rheological properties included in the model are regarded as *effective* parameters for water-soluble surfactants. However, very few attempts have been made to draw a quantitative comparison between those models including surface rheology and experimental data available on thin films formed from water-soluble surfactant solutions; see references^{26,34} for LLD configuration and reference⁵ for Frankel configuration.

Delacotte *et al.*¹² have measured the thickness of the film coated on a solid plate as a function of the plate velocity for the non-ionic surfactant $C_{12}E_6$ at various concentrations (symbols in figure 2a). Similar measurements have been performed by Saulnier *et al.*¹⁸ on free films, using the same surfactant and concentrations as Delacotte *et al.* (symbols in figure 2b). Both authors observe a deviation from the $Ca^{2/3}$ behavior at high capillary numbers and propose a qualitative explanation based on the idea, developed by Prins *et al.*³⁵ and Lucassen *et al.*³², that the ability of the liquid/air interfaces of a film to sustain surface tension gradients decreases with film thickness. The authors thus argue that, at low capillary numbers, the film is so thin that it does not contain enough surfactants to replenish the surface when the latter is stretched: a liquid/air interface then behaves as if it were rigid. On the contrary, at higher capillary numbers, the film should be thick enough so that surface tension gradients could be partly compensated by surfactant adsorption at the liquid/air interfaces. The observed deviation would then be due to a “reservoir effect”, as named by Quéré²¹. Relying on their work, we propose in this article to rationalize quantitatively the deviations from Frankel and LLD laws observed at high capillary numbers in a unified description in terms of surface elasticity E defined as³⁶

$$E = A \frac{\partial \gamma}{\partial A}, \quad (4)$$

where A is the area of the liquid/air interface and γ is the surface tension. To our knowledge, this is the first quantitative comparison between a model including surfactant dynamics and experiments in both LLD and Frankel configurations.

In section II, the different regimes exhibited by the data in figure 2 and the corresponding transitions are discussed in terms of scaling laws. “Twin” models, coupling the hydrodynamics and the dynamics of insoluble surfactants at the liquid/air interfaces, are then recalled in section III and numerically solved for soap films as well as for coated films. Quantitative comparison between models and experiments is finally performed: suprisingly, we find that the data can be well described assuming a *constant* surface elasticity, as will be discussed in section IV.

II. SCALING ANALYSIS

A. Partially rigid interfaces

The typical lengthscales in the x - and y -directions (defined in figure 1) are respectively given by the lengthscale ℓ of the transition region – called the dynamic meniscus – which connects the static meniscus to the flat part of the film, and the thickness h_0 of the film far from the liquid bath. The lengthscale $\ell \sim \sqrt{h_0 \ell_c}$ is obtained from the curvature matching condition between the dynamic and static menisci

$$\partial_{xx}h = \frac{\sqrt{2}}{\ell_c} \quad \text{for } x \rightarrow -\infty \quad (5)$$

and is typically of the order of $20 - 200 \mu\text{m}$ in the range of Ca explored experimentally ($\text{Ca} = 10^{-6} - 10^{-3}$). If the vertical velocity u is taken to scale like the pulling velocity V and the pressure P , assumed to be uniform across the film, like the capillary pressure in the static meniscus γ_0/ℓ_c , eq. (1) can be recovered (with $K = 1$) from the scaling analysis of the x -component of Stokes equations:

$$\eta \partial_{yy}u = \partial_x P. \quad (6)$$

As soon as we want to refine the boundary condition at the liquid/air interface, *i.e.* to explore intermediate cases between the fluid and rigid limits, the balance of tangential forces at the liquid/air interface has to be considered:

$$\eta \partial_y u|_{y=h(x)} = \partial_x \gamma. \quad (7)$$

The viscous stress at the interface $\eta \partial_y u|_{y=h(x)}$ can be computed by integrating (6) along y between 0 and $h(x)$, so that eq. (7) becomes

$$\eta \partial_y u|_{y=0} + h \partial_x P = \partial_x \gamma, \quad (8)$$

where the surface tension gradient $\partial_x \gamma$ scales like E/ℓ and the film thickness h (or half the film thickness in the case of a soap film) like h_0 .

We have chosen here to describe the intermediate cases between the fluid and rigid limits using surface elasticity E to quantify the stress at the interface. This is equivalent to a description in terms of surface velocity u_s , as pictured in figure 3. For small surface elasticities, the stress at the interface vanishes and the interfacial velocity u_s is non-zero: we recover the fluid case. For larger surface elasticities, the stress at the interface is large and the surface velocity u_s is approaching V : we recover the rigid case.

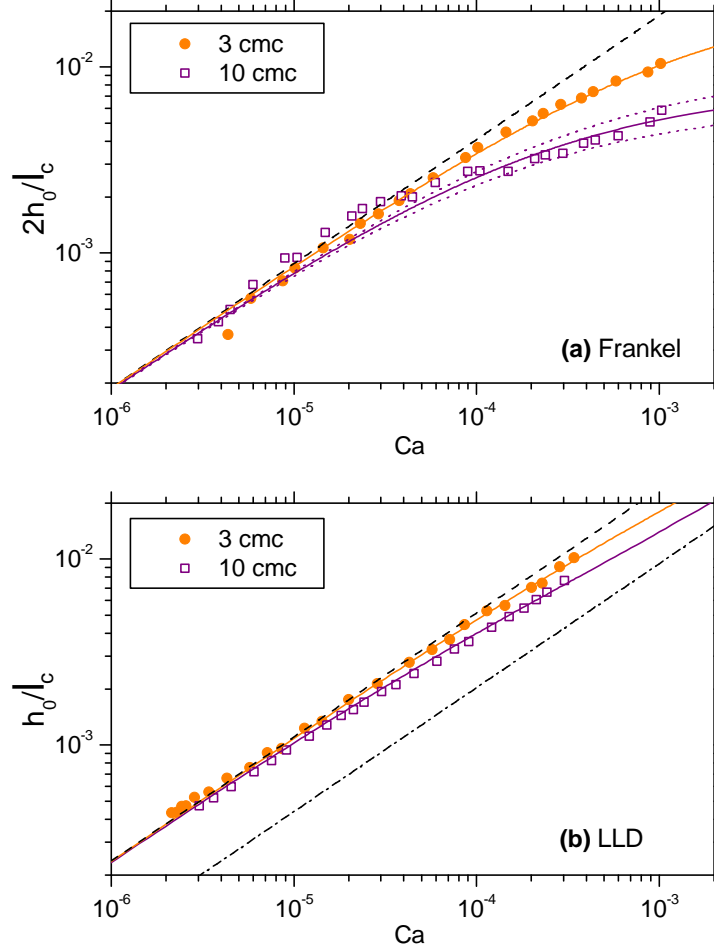


FIG. 2. (a) Frankel configuration: the film thickness $2h_0$ normalized by the capillary length ℓ_c is plotted as a function of the capillary number Ca . Symbols correspond to experimental data for soap films pulled from $C_{12}E_6$ solutions of two different concentrations³⁷, respectively 3 and 10 times the critical micellar concentration (cmc). Solid lines are fits of the experimental data using the model described in section III, where the only adjustable parameter is the (effective) surface elasticity E . The dotted lines give an estimation of the maximal error on the fit, and thus on the numerical value of surface elasticity (see later). Finally, the dashed line corresponds to Frankel's law (eq. (1) with K_{Fr}), namely the limit of totally rigid liquid/air interfaces. — (b) LLD configuration: same as (a) for coated films entrained from $C_{12}E_6$ solutions¹² at the same concentrations as in Frankel configuration. The dashed line corresponds to the LLD law in the limit of a totally rigid liquid/air interface (eq. (1) with K_{LLD}^{rigid}) and the dash-dotted line to the limit of a fluid liquid/air interface (eq. (1) with K_{LLD}^{fluid}).

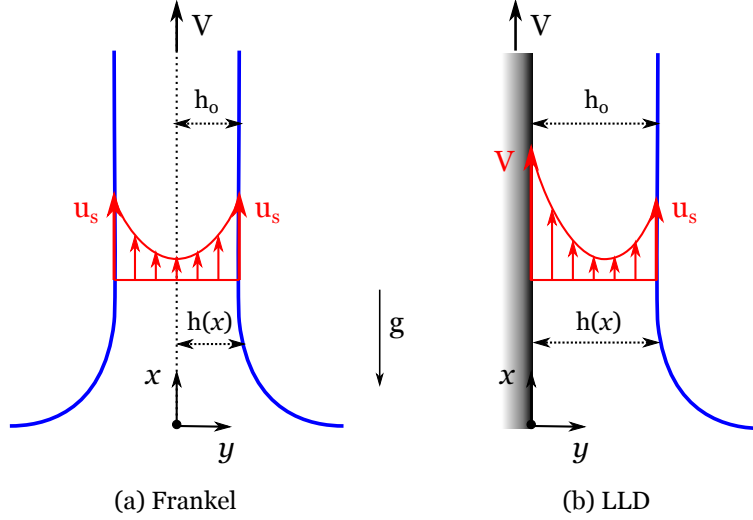


FIG. 3. Sketches of the vertical velocity field $u(x, y)$ for (a) Frankel configuration and (b) LLD configuration in the case of *partially* rigid liquid/air interfaces. The interfacial velocity $u_s(x)$ is introduced to account for finite surface elasticity. All velocities are defined in the reference frame of the laboratory.

B. Frankel configuration

When considering a soap film with partially rigid interfaces, it is no longer clear that the vertical velocity u scales like V , since the interfacial velocity u_s introduces a second velocity scale, which is *a priori* different from V . However, thanks to the symmetry of the film with respect to the vertical axis, $\partial_y u|_{y=0}$ vanishes in eq. (8) in the case of Frankel configuration, leading to the velocity-independent equation

$$\partial_x \gamma = h \partial_x P, \quad (9)$$

where the left-hand side represents the elastic (Marangoni) force dragging liquid up, while the right-hand side is the capillary suction driving liquid down. From this equation we can draw a velocity-independent scaling law for h_0 :

$$h_0 \sim \ell_c \frac{E}{\gamma_0}. \quad (10)$$

In the case of partially rigid interfaces, the thickness of a soap film is thus found to scale independently of the pulling velocity. Such a velocity-independent regime was already identified by Scheid *et al.*⁸ in the case of surface tension gradients induced by thermocapillary effects. It was also obtained in the context of thin films pulled from surfactant-polymer mixtures by Bruinsma *et al.*⁷. The transition between this velocity-independent regime, corresponding to partially rigid interfaces, and Frankel's regime, corresponding to totally rigid interfaces, is found by comparing eq. (10) to the scaling of Frankel's law (eq. (1)). Defining the Marangoni number as $\text{Ma} = E/\gamma_0$, this transition occurs for

$$\text{Ca}^* \sim \text{Ma}^{3/2}. \quad (11)$$

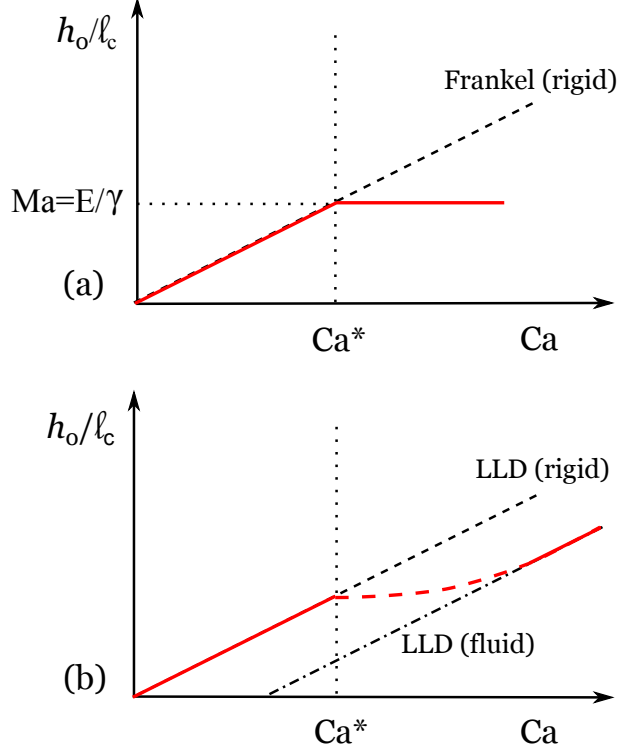


FIG. 4. Sketches of the velocity (or equivalently capillary number) dependence of film thickness for (a) Frankel configuration and (b) LLD configuration, obtained by scaling analysis. When considering partially rigid liquid/air interface in Frankel configuration (a), a velocity-independent regime is expected at high capillary numbers ($Ca > Ca^*$ given by eq. (11)), whereas Frankel's law (1), assuming perfectly rigid interfaces, remains valid at lower capillary numbers. When considering partially rigid liquid/air interface in LLD configuration (b), we recover the limit of the LLD model with totally *fluid* interfaces at high capillary numbers $Ca \gg Ca^*$. A transition regime, which cannot be simply described in terms of a scaling law, is expected for $Ca \gtrsim Ca^*$. Finally, the LLD model with totally *rigid* interfaces should be recovered for $Ca < Ca^*$.

Figure 4a summarizes this scaling analysis for Frankel configuration. Experimental data (figure 2a) show that low capillary numbers ($Ca < Ca^*$) correspond to Frankel's regime. On the contrary, the film thickness seems to converge, without reaching it, towards a velocity-independent regime at high capillary numbers ($Ca \gg Ca^*$). An order of magnitude for the critical capillary number at which the transition occurs can be estimated from figure 2a: for $C_{12}E_6$ solutions at concentrations 3 and 10 cmc, we find $Ca^* \sim 10^{-4}$.

This brings evidence that the "rigidity" of liquid/air interfaces cannot be considered as a property of the surfactant solution. We indeed show that, at a given position on the film, the mechanical behaviour of the liquid/air interfaces of a free film can range from rigid (*i.e.* well described by Frankel's law) to partially rigid upon increasing the pulling velocity.

C. LLD configuration

In the LLD configuration, the symmetry of the film with respect to the vertical axis is lost and the $\partial_y u|_{y=0}$ term in eq. (8) must be kept. However, the no-slip condition at the solid/liquid interface ensures that, in the case of a partially rigid (or even fluid) boundary condition at the liquid/air interface, V remains the right velocity scale for u . In the end, using the scaling of eq. (5) to compute ℓ , all terms in eq. (8) can be estimated:

$$\underbrace{-\eta \partial_y u|_{y=0}}_{\sim \frac{\eta V}{h_0}} + \underbrace{\partial_x \gamma}_{\sim \frac{E}{\sqrt{\ell_c h_0}}} = \underbrace{h(x) \partial_x P}_{\sim \gamma_0 \left(\frac{h_0}{\ell_c^3}\right)^{1/2}}. \quad (12)$$

In the limit of a partially rigid liquid/air interface ($u_s < V$), equation (12) expresses the balance between the forces that pull the film upwards (left-hand term) and the capillary suction, which drives liquid downwards (right-hand term). The left-hand term of eq. (12) is the sum of two contributions: the viscous entrainment plus the surface elastic contribution associated to surface tension gradients. If this term is dominated by the viscous entrainment contribution, we recover the classical LLD law in the *fluid* limit, namely with prefactor $K_{\text{LLD}}^{\text{fluid}}$ and $u_s \ll V$. Upon decreasing the capillary number, the (surface) elastic contribution can become of the order of the viscous entrainment contribution. This intermediate regime, which occurs around the critical capillary number Ca^* given by eq. (11), cannot be simply described by a scaling law. For even lower capillary numbers, we expect to observe a transition towards the *rigid* limit, namely LLD law with prefactor $K_{\text{LLD}}^{\text{rigid}} = 4^{2/3} K_{\text{LLD}}^{\text{fluid}}$ and $u_s = V$. The fluid and rigid limits, as well as the transition, are sketched in figure 4b, although both limits have not been observed together for a given surfactant concentration. For a given surfactant concentration, it is indeed the value of surface elasticity that determines which portion of the curve sketched in figure 4b is observed in the range of capillary numbers where our hypotheses (no gravitational drainage, no inertia) are valid.

III. HYDRODYNAMIC MODEL INCLUDING SURFACE ELASTICITY

A. Hypotheses and governing equations

Although the experimental results were obtained with water-soluble surfactants, we will try to describe them using a model for water-insoluble surfactants in the spirit of references^{5,27}. In that framework, the general definition of surface elasticity (eq. (4)) boils down to

$$E = -\Gamma \frac{\partial \gamma}{\partial \Gamma}, \quad (13)$$

where Γ is the surface concentration of surfactants. For soluble surfactants, E is *a priori* a function of the surface concentration Γ , of the film thickness (due to reservoir effects²¹) and possibly of the generation velocity, which determines the timescale to be compared to the adsorption time of surfactants at the liquid/air interfaces. In the following, we however make the strong assumption (to be discussed later) that E is constant, so that eq. (13) can be integrated to find the equation of state

$$\gamma(\Gamma) = \gamma_0 - E \ln \left(\frac{\Gamma}{\Gamma_0} \right), \quad (14)$$

with $\gamma_0 = \gamma(\Gamma_0)$ the surface tension in the liquid bath (far from the film) and Γ_0 the corresponding surface concentration. Note that this equation of state differs from the one used in references^{5,27}, which was the linearized equation of state obtained when assuming that Γ stays close to Γ_0 . However, the results presented in subsection IV D show that this hypothesis is not valid anymore at high capillary numbers (namely for $\text{Ca} \gtrsim 10^{-4}$). Detailed comparison between the solutions obtained using the linearized and non-linearized equations of state is discussed in appendix A.

Like for deriving Frankel's and LLD laws, we assume stationarity and the existence of a region where the film thickness is uniform, far from the liquid bath, and equals to h_0 . Surface diffusion is neglected and all equations are written at leading order in the frame of the lubrication approximation, *i.e.* $h_0/\ell \ll 1$, corresponding to small interfacial slopes ($\partial_x h \ll 1$). Under those assumptions, the film thickness $h(x)$ (or half the film thickness for a soap film), the vertical velocity $u(x, y)$, the vertical surface velocity $u_s(x) = u(x, h(x))$, the pressure $P(x, y)$ and the surface concentration of surfactants $\Gamma(x)$ obey the following system of coupled differential equations:

- Lubrication equations:

$$\begin{aligned} \partial_x P &= \eta \partial_{yy} u, \\ \partial_y P &= 0, \end{aligned} \tag{15}$$

- Normal force balance at the liquid/air interface:

$$P(x, y = h(x)) = P_0 - \gamma \partial_{xx} h, \tag{16}$$

- Tangential force balance at the liquid/air interface:

$$\eta \partial_y u|_{y=h(x)} = \partial_x \gamma, \tag{17}$$

- Conservation of surfactant number at the liquid/air interface:

$$\partial_x (u_s \Gamma) = 0, \tag{18}$$

- Mass conservation in the bulk of the film:

$$\partial_x (\bar{u} h) = 0, \tag{19}$$

where

$$\bar{u}(x) = \frac{1}{h(x)} \int_0^{h(x)} u(x, y) dy, \tag{20}$$

is the average velocity in the film (or half the film for a soap film) at a given height x .

In the following, we give the non-dimensionalized differential systems to be solved and we refer the interested reader to references^{5,27} for the details of the derivation in the LLD and Frankel configurations respectively. The only differences in our model are:

- i) the equation of state (14), which remains nonlinear,
- ii) the correction to the capillary pressure gradient due to the variation of surface tension, which was accounted for in ref.²⁷ but not in ref.⁵.

The influence of these choices on the results will be discussed later in the text and in appendix A.

B. Frankel configuration

The pressure and velocity fields are eliminated from the previous system, leaving three one-dimensional fields $h(x)$, $u_s(x)$ and $\Gamma(x)$ to be determined. The equations are non-dimensionalized as follows: y and h are rescaled by h_0 , x by ℓ , γ by γ_0 , u_s by V and Γ by Γ_0 . We also define the aspect ratio $\epsilon = h_0/\ell \ll 1$, which scales the interfacial slope $\partial_x h$. Considering that the dominant balance is capillary suction versus viscous entrainment, *i.e.* the scaling of h_0 is still given by Frankel's law (1), leads to $\epsilon = \text{Ca}^{1/3}$, as discussed in reference¹⁰. Finally, the non-dimensionalized system to be solved, using a prime to denote x -derivatives, is:

- Differential equation for the film thickness $h(x)$:

$$h''' = 3 \frac{(1 - u_s h)}{\gamma h^3} + \text{Ma} \frac{h''}{\gamma} \frac{\Gamma'}{\Gamma} \approx 3 \frac{(1 - u_s h)}{\gamma h^3}, \quad (21)$$

- Differential equation for the surface velocity $u_s(x)$:

$$u_s' = -3\Lambda \frac{u_s}{h^2} (1 - u_s h), \quad (22)$$

- Differential equation for the surface concentration $\Gamma(x)$:

$$\Gamma' = -\frac{\Gamma}{u_s} u_s', \quad (23)$$

- Equation of state

$$\gamma(\Gamma) = 1 - \text{Ma} \ln(\Gamma) \approx 1, \quad (24)$$

where we have defined the dimensionless parameter Λ as

$$\Lambda = \frac{\text{Ma}}{\text{Ca}^{2/3}}. \quad (25)$$

We take $x = 0$ a position in the flat region of the film (far from the liquid bath) and $x = -L$ the position where the asymptotic matching between the dynamic and static meniscii is made. Note that the solutions do not depend on L as long as it is large enough, so that the curvature $h''(-L)$ has converged towards a constant value, denoted $h''(-\infty)$. The non-dimensionalized boundary conditions then read: $h(0) = 1$, $h'(0) = 0$, $h''(0) = a$, $u_s(0) = 1$ and $\Gamma(-L) = 1$, with a an infinitesimally small parameter (here $a = 10^{-3}$).

The solid lines displayed in figure 2a have been obtained solving the above system under the assumption that $\text{Ma} \ll 1$, so that the Marangoni term in equations (21) and (24) can be neglected. We shall justify this assumption in appendix A, where we compare the solution obtained by solving the whole system to the one derived from the approximated system. In the case of soap films, we show that the above approximation remains correct as long as $\text{Ma} \lesssim 0.1$. In the end, this leaves us with a single parameter, Λ , that controls the solutions of the system. It is worth noting that the critical capillary number Ca^* identified in the scaling analysis (section II) corresponds to $\Lambda \sim 1$. This brings evidence that Λ is indeed the natural parameter to describe the transition between the limits of totally rigid and partially fluid liquid/air interfaces.

C. LLD configuration

Following the same steps as in Frankel configuration, the LLD geometry leads to the following system of non-dimensionalized equations:

- Differential equation for the film thickness $h(x)$:

$$h''' = 6 \frac{[2 - (1 + u_s)h]}{\gamma h^3} + \text{Ma} \frac{h''}{\gamma} \frac{\Gamma'}{\Gamma} \approx 6 \frac{[2 - (1 + u_s)h]}{\gamma h^3}, \quad (26)$$

- Differential equation for the surface velocity $u_s(x)$:

$$u'_s = -2\Lambda \frac{u_s}{h^2} [3 - (1 + 2u_s)h], \quad (27)$$

- Differential equation for the surface concentration: eq. (23),
- Equation of state: eq. (24).

The non-dimensionalized boundary conditions are the same as in Frankel configuration. Similarly, the solid lines displayed in figure 2b have been obtained solving the above system under the assumption that $\text{Ma} \ll 1$, so that the Marangoni term in equations (26) and (24) can be neglected. In the case of coated films, we show in appendix A that this approximation remains correct as long as $\text{Ma} \lesssim 0.01$. As in Frankel configuration, we are left with a single control parameter Λ , defined in eq. (25).

IV. RESULTS AND DISCUSSION

A. Film thickness versus capillary number

The systems of equations described in subsections IIIB and IIIC are solved numerically using the continuation software AUTO-07p³⁸, for different values of the dimensionless parameter Λ . For a given Λ and a given Ma , we compute the actual film thickness h_0 (or half the film thickness in the case of a soap film) in the flat part of the film using the curvature matching condition eq. (5) in its dimensionless form (for $x \rightarrow -\infty$):

$$\frac{h_0}{\ell_c} = \frac{h''(-\infty)}{\sqrt{2}} \text{Ca}^{2/3}. \quad (28)$$

Setting a numerical value for the Marangoni number Ma , we are able to deduce h_0 as a function of the capillary number $\text{Ca} = (\text{Ma}/\Lambda)^{3/2}$ from the mastercurve $h_0(\Lambda)$. For Frankel (resp. LLD) configuration, we thus have a family of theoretical curves $h_0(\text{Ca})$ parametrized by Ma , as illustrated in figure 5a (resp. 5b). In the case of soap films (figure 5a), the theoretical curves $h_0(\text{Ca})$ superimpose on Frankel's prediction (dashed line) at “low” capillary numbers and then deviate from it around a critical capillary number that increases with Ma . All these features are consistent with the qualitative behavior predicted from the scaling analysis (figure 4a). Note that no velocity-independant regime is truly reached at “high” capillary numbers in the range of Ca and Ma relevant for experiments. In the case of coated films (figure 5b), the rigid limit (dashed line) is also recovered at “low” capillary numbers. As expected from the scaling analysis, the larger the Marangoni number, the larger the critical capillary number at which the transition towards the fluid limit begins. However, the fluid limit itself is not recovered at “high” capillary numbers because of a loss a convergence of numerical solutions in this domain of parameters, as detailed in appendix A.

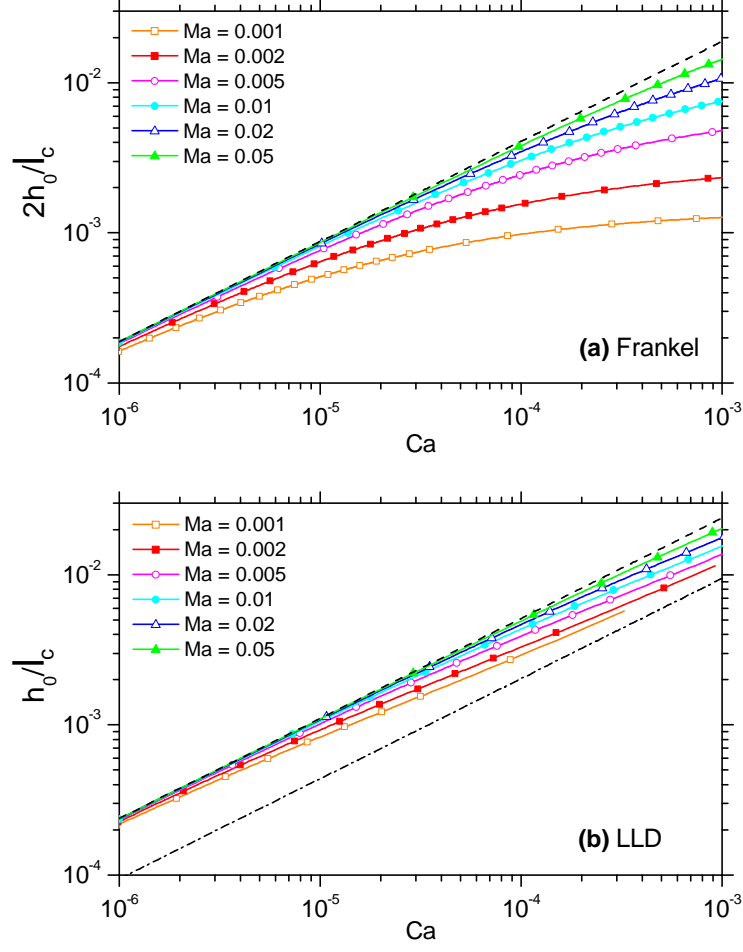


FIG. 5. (a) Frankel configuration: the predicted film thickness $2h_0$ normalized by the capillary length ℓ_c is plotted as a function of the capillary number Ca . Different symbols/colors correspond to different values of the Marangoni number Ma . The dashed line corresponds to Frankel's law, namely the limit of totally rigid liquid/air interfaces. — (b) LLD configuration: same as (a) for the coated film thickness h_0 . The dashed line corresponds to the LLD law for the limit of a totally rigid liquid/air interface and the dash-dotted line to the limit of a fluid liquid/air interface.

B. From experimental data to surface elasticity

For practical use, a non-linear fit of the mastercurve $h_0(\Lambda)$ is proposed in appendix B in both Frankel and LLD configurations. We can then draw an analytical expression of h_0 as a function of the capillary number $Ca = (Ma/\Lambda)^{3/2}$, where Ma is the only adjustable parameter. This expression is used to fit the experimental data available on soap (resp. coated) films pulled from $C_{12}E_6$

	C ₁₂ E ₆	3 cmc	10 cmc
Frankel	Ma $\times 10^3$	18 $^{+8}_{-2}$	5.6 $^{+1.4}_{-1.2}$
	E (mN/m)	0.62 $^{+0.28}_{-0.07}$	0.19 $^{+0.05}_{-0.04}$
LLD	Ma $\times 10^3$	22 $^{+8}_{-7}$	5.6 $^{+1.4}_{-2.1}$
	E (mN/m)	0.71 $^{+0.26}_{-0.23}$	0.18 $^{+0.05}_{-0.07}$

TABLE I. Summary of the fitted Marangoni numbers Ma obtained for free standing and coated films pulled from C₁₂E₆ solutions of concentration 3 cmc and 10 cmc (see figure 2). The corresponding surface elasticity $E = \gamma_0 \text{Ma}$ was then deduced taking the experimental values for surface tension $\gamma_0 = 34.5$ mN/m for Frankel configuration¹⁸ and $\gamma_0 = 32.3$ mN/m for LLD configuration¹². The confidence interval on the Marangoni number was estimated from the upper and lower values associated to “reasonable” fits of the data, as illustrated by the dotted lines in figure 2a for 10 cmc.

solutions (symbols in figure 2) and extract a value for Ma. The best fits are shown in figure 2 (solid lines) for two different surfactant concentrations above the critical micellar concentration (cmc). The corresponding values for the Marangoni number Ma and surface elasticity E are summarized in table I.

The main result of table I is that the experimental data for both Frankel and LLD configurations can be rationalized by the *same* value of surface elasticity for a given surfactant concentration. This brings evidence that surface elasticity – in the effective sense we consider here when comparing experimental data for water-soluble surfactants to an insoluble-surfactant model – is an intrinsic property of a surfactant solution (*e.g.* independant of the pulling velocity and on the configuration). Together with the fitting equations proposed in appendix B, the Frankel and LLD experiments can thus be used more systematically as surface rheometers by extracting the value of the effective surface elasticity from experimental curves $h_0(\text{Ca})$. Applying this method to the data obtained by Delacotte *et al.*¹² on C₁₂E₆ and C₁₂TAB coated films, and by Saulnier *et al.*^{18,37} on C₁₂E₆ and SDS soap films, we have been able to obtain surface elasticity as a function of surfactant concentration (above the cmc) for different surfactants, as presented in figure 6.

C. Discussion of the results on surface elasticity

In spite of the strong hypothesis of a constant surface elasticity, the model is in surprisingly good agreement with the experimental data, as shown in figure 2. Two factors would indeed be expected to play a role in the dependency of E on the capillary number: i) the reservoir effect, changing the local surfactant concentration in the film depending on the film thickness, and ii) the timescale of surfactant adsorption at the liquid/air interfaces.

- i) *Reservoir effect* — Prins *et al.*³⁵ showed that the surface elasticity decreases when the film thickness increases, which has been interpreted as a reservoir effect²¹. The local surfactant concentration in thin films is thought to be much lower than the bulk concentration: since they lack surfactant molecules to populate a newly-created interface, thin films thus sustain surface tension gradients better than thicker films do. However, the data can be fitted using a single value of surface elasticity over the whole range of capillary numbers probed in the experiments ($\text{Ca} = 10^{-6} - 10^{-3}$). We have shown that the relevant control parameter for the rigidity of liquid/air interfaces is $\Lambda = \text{Ma}/\text{Ca}^{2/3}$. Hence, even for low values of the Marangoni

		τ_{ads}	c	Reference
SDS	Short time	6 ms	4 cmc	Owens <i>et al.</i> ⁴²
	Long time	10 s	1 cmc	Henderson <i>et al.</i> ⁴³
C ₁₂ TAB	Short time	< 10 ms	1 cmc	Ritacco <i>et al.</i> ⁴¹
	Long time	2 s	1 cmc	Ritacco <i>et al.</i> ⁴¹

TABLE II. Summary of experimental values of adsorption times found in the literature for the anionic surfactant SDS and the cationic surfactant C₁₂TAB, to be compared to the characteristic timescale τ of the experiments. The “short time” is the time needed by the surfactants in the subsurface to diffuse up to the bare surface, whereas the “long time” corresponds to the time required by these surfactants to adsorb onto the surface when it is already populated, *i.e.* to overcome the corresponding electrostatic adsorption barrier.

number (low surface elasticities), the liquid/air interfaces can exhibit a rigid behavior provided the capillary number is sufficiently small ($\text{Ca} \lesssim 5 \times 10^{-5}$ for the data displayed in figure 2). Due to the contribution of reservoir effects, the actual value of surface elasticity at these low capillary numbers may be larger than the one we computed, but this contribution cannot be distinguished since the value of Λ is already high enough, so that the interfaces behave as rigid. On the contrary, at higher capillary numbers, *i.e.* for thicker films, the contribution of reservoir effects becomes less and less important and apparently does not affect much the value of surface elasticity, since a constant surface elasticity fits well the data.

- ii) *Adsorption timescale* — The typical timescale τ in Frankel and LLD experiments can be defined as the time spent by surfactants in the dynamic meniscus, where the surface is stretched, namely $\tau = \ell/V$. This timescale, which lies in the range 3 – 600 ms for the experimental data discussed here, is to be compared to the characteristic adsorption time of surfactants at the liquid/air interface, denoted τ_{ads} . For the non-ionic surfactant C₁₂E₆, the adsorption is purely diffusion-limited³⁹ and τ_{ads} is found experimentally⁴⁰ to be of the order of 100 s for a bulk concentration $c = 10$ cmc. We thus have $\tau \ll \tau_{\text{ads}}$ for C₁₂E₆ for the whole range of capillary numbers probed, hence a negligible contribution of adsorption effects to the variation of surface elasticity in this case. The estimation of an adsorption time is a different matter for the ionic surfactants SDS and C₁₂TAB, for which short time adsorption is essentially controlled by diffusion, whereas long time behavior depends on electrostatic adsorption barriers⁴¹. The orders of magnitude presented in table II essentially show that even though the timescale τ of the experiments is large compared to the diffusion time, τ is still small compared to the time needed for the surfactants to overcome the electrostatic adsorption barrier. For non-ionic as well as for ionic surfactants, the timescale separation might explain why the effective surface elasticity appears to be independant of Ca . Note that the above discussion on timescales is modified if the surfactant concentration in the film is different from the surfactant concentration in the bulk of the solution due to reservoir effects.

Prins *et al.*³⁵ have measured surface elasticity (note that there is a factor 2 in their definition of E , compared to ours) as a function of film thickness for a solution of SDS at a concentration of 3 times the cmc. Their values of E lie in the range 0.45 – 1.2 mN/m and are in good agreement with the value $0.79^{+0.26}_{-0.23}$ mN/m (see figure 6) we obtain with the same solution. To our knowledge, direct measurements of surface elasticity in thin films, such as Prins’s, do not exist for C₁₂E₆, nor for C₁₂TAB. Nonetheless, the surface elasticities of C₁₂E₆ and C₁₂TAB solutions have respectively

been measured using a dynamic drop tensiometer³⁶ and the capillary waves method⁴⁴, but only up to bulk concentrations of 1 cmc. Comparison to our results is then hardly possible, all the more so that the above-mentioned experimental techniques do not take reservoir effects into account, and involve a timescale (set by the excitation frequency) which is difficult to relate to Frankel and LLD experiments.

Soap film pulling and plate coating experiments have finally proved to be reliable surface rheometers to measure values of surface elasticity that are of the order or smaller than the resolution limit of classical devices (around 1 mN/m), such as Langmuir troughs or rising bubble techniques. This surface elasticity is to be considered as an effective parameter that somehow also includes the reservoir effect specific to thin films and the dynamics of surfactant adsorption at the liquid/air interfaces. It should be stressed that, although those effects do not influence visibly the *variation* of surface elasticity in the range of Ca probed experimentally, they certainly do contribute to the numerical *value* of E .

Additionally, the two effects discussed above support *a posteriori* the use of a model designed for insoluble surfactants: either because of the reservoir effect and/or because the timescale of adsorption is larger than the typical timescale of the experiment, the water-soluble surfactants behave here as if they were water-insoluble.

D. Surface tension gradient

For a given Λ , the (dimensionless) surface concentration $\Gamma(0)$ in the flat part of the film is obtained from the resolution of the models. For the particular values of Ma displayed in table I, the relative surface concentration variation between the liquid bath and the flat part of the film, defined as $\Delta\Gamma = 1 - \Gamma(0)$, is computed as a function of the capillary number Ca, for Frankel (figure 7a) and LLD (figure 7b) configurations.

The relative surface concentration difference $\Delta\Gamma$ between the flat part of the film and the liquid bath increases with the capillary number for both Frankel and LLD configurations, and eventually becomes of the order of unity. This shows that the linearization of the equation of state (14) is no longer justified for high capillary numbers ($\text{Ca} \gtrsim 10^{-4}$) and introduces biases that are discussed in details in appendix A.

For a given Marangoni number Ma, we are able to compute the (dimensionless) surface tension $\gamma(x=0)$ in the flat part of the film from the equation of state eq. (24). The relative surface tension variation between the liquid bath and the flat part of the film, defined as $\Delta\gamma = \gamma(x=0) - 1$, is then plotted as a function of the capillary number Ca for Frankel (figure 7c) and LLD (figure 7d) configurations, for the particular values of Ma given in table I.

The relative surface tension difference $\Delta\gamma$ between the flat part of the film and the liquid bath is found to increase with the capillary number for both Frankel and LLD configurations, but does not reach more than a few percents in the range of capillary numbers probed experimentally. Numerically, this corresponds to a surface tension difference $\Delta\gamma \approx 0.2$ mN/m for a soap film pulled from a C_{12}E_6 solution at 3 cmc at a typical velocity $V \approx 2$ mm/s ($\text{Ma} \approx 0.022$, $\text{Ca} \approx 6 \times 10^{-5}$). This order of magnitude is consistent with theoretical results obtained by Seiwert *et al.*⁵ for Frankel configuration, as well as with *in situ* surface tension measurements performed by Caps *et al.*⁴⁵ in a soap film.

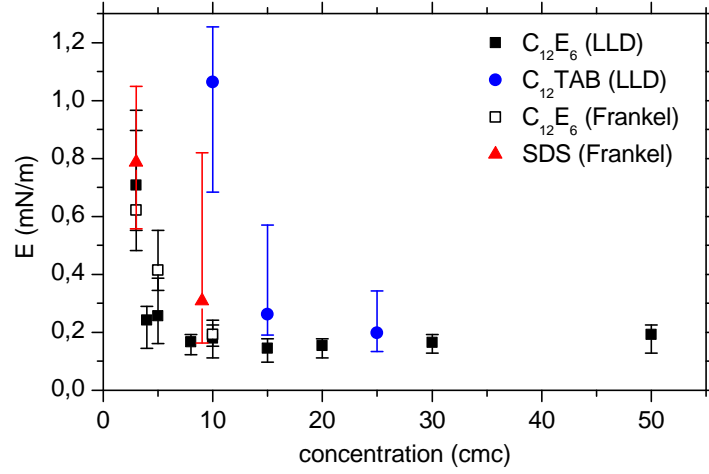


FIG. 6. The (effective) surface elasticity E is plotted as a function of surfactant concentration (counted in number of cmc) for the non-ionic surfactant $C_{12}E_6$, the cationic surfactant $C_{12}TAB$ and the anionic surfactant SDS. The values of elasticity have been obtained by fitting the corresponding experimental curves $h_0(Ca)$, either in Frankel^{14,37} or in LLD¹² configuration, using the model described in section III C. The error bars stand for the maximal error on E deduced from the confidence interval on the Marangoni number (details can be found in the caption of table I).

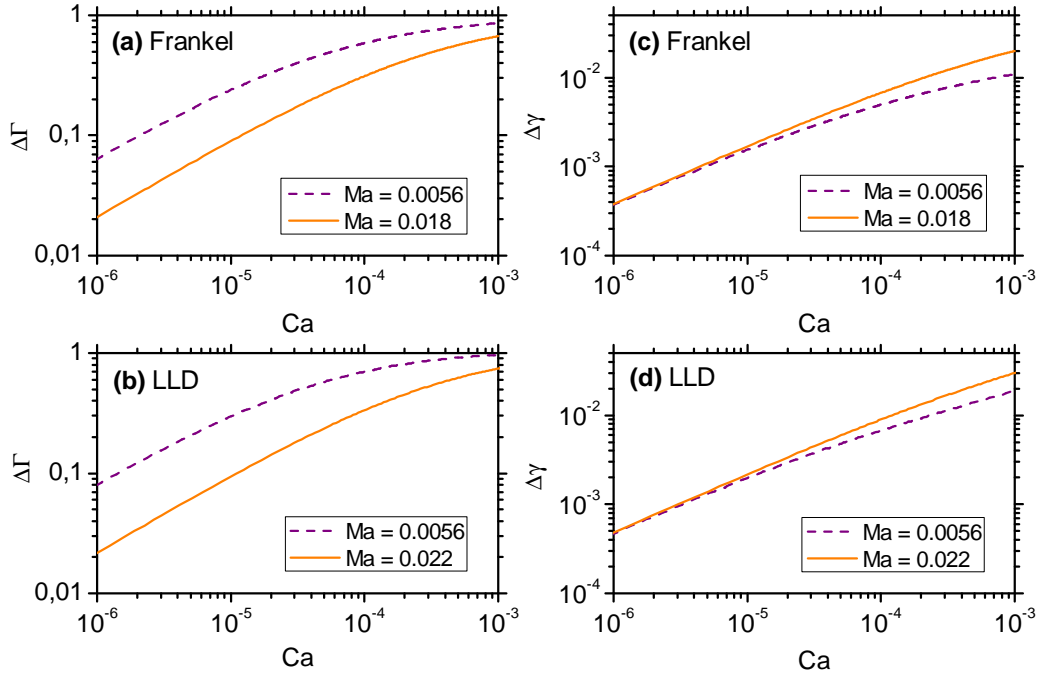


FIG. 7. The dimensionless surface concentration difference $\Delta\Gamma$ and the dimensionless surface tension difference $\Delta\gamma$ between the flat part of the film and the liquid bath are plotted as functions of the capillary number Ca for (a), (c) Frankel configuration and (b), (d) LLD configuration. In all cases, the Marangoni number Ma has been set to the value extracted from the fit of the corresponding experimental data (see table I).

V. CONCLUSION

We have presented two equivalent hydrodynamical models including surface elasticity, for soap film pulling and plate coating experiments, respectively. This is to our knowledge the first quantitative comparison between free standing and coated films since the pioneering work by Frankel on the one hand, and Landau, Levich and Derjaguin on the other hand.

The predictions of the models, assuming water-insoluble surfactants, are compared to experimental data available for soap and coated films stabilized by the water-soluble surfactant $C_{12}E_6$ to extract a value for surface elasticity. In this context, surface elasticity is to be understood as an “effective” quantity, incorporating the contributions of the reservoir effect in thin films, as well as the adsorption dynamics of surfactants at the liquid/air interfaces. For a given surfactant concentration, both Frankel and LLD configurations independently yield the same value for the effective surface elasticity, proving that it is an intrinsic property of a surfactant solution. Hence coating or film pulling experiments can be used in practice, together with the results of the models presented in this article (see appendix B), to measure the effective surface elasticity of surfactant solutions, especially for low elasticity values which are unmeasurable with classical techniques (*e.g.* Langmuir troughs or rising bubble experiments). Additionally, we were able to predict the surface tension difference between the liquid bath and the flat part of the film as a function of the capillary number.

A soap film during its generation exhibits two distinct zones¹⁸: the upper part, where the thickness decreases with time, was recently studied by Saulnier *et al.*⁴⁶; the lower part, which has a constant and uniform thickness, is described in the present work. Combining the results of both studies, it is now possible to get a prediction for the surface tension difference across the whole film. For a $C_{12}E_6$ solution at 3 cmc and $Ca \approx 6 \times 10^{-5}$, this total surface tension difference is of the order of $1 - 2$ mN/m, which is small compared to the surface tension of usual solutions, but well in line with other recent theoretical and experimental work on surface tension gradients in soap films^{5,45}.

As a consequence of our analysis, it is found that the “rigidity” of a liquid/air interface, *i.e.* the nature of the boundary condition at this interface, *cannot* be considered as a property of the surfactant solution. Saulnier *et al.*⁴⁶ already demonstrated that the upper part of the film is well described by a fluid (no shear) boundary condition, whereas its lower part obeys Frankel’s law for $Ca < Ca^*$, showing that rigid interfaces are a good approximation in that zone. Similarly, we have shown here that, for a given solution, the pulling velocity dependency of the film thickness is rationalized only when considering that the mechanical behaviour of the liquid/air interfaces ranges from totally to partially rigid upon increasing the pulling velocity. This change in the boundary condition stems from a change in the relative contributions of viscous and elastic entrainments to the force balance. Our work thus shows that the paradigm of a $2/3$ power law in Ca , used to fit experimental film thickness for both Frankel and LLD configurations by many different authors and for decades, might well be obsolete in the case of films containing surface active agents.

Although we have been focusing here on a plane geometry, the work presented in this paper could in principle be extended to other geometries, like fiber coating^{21,22,47} or bubbles moving in capillaries²³, provided the curvature of the static meniscus $\sqrt{2}/\ell_c$ appearing in the matching condition (5) is replaced by $1/r$, where r is either the fiber radius or the capillary radius.

Appendix A: Comparison of linearized and non-linearized equations of state

In this section, we discuss some assumptions we have made in the models presented in sections IIIB and IIIC. Unlike in references^{5,27}, we have kept the non-linearized form of the equation of

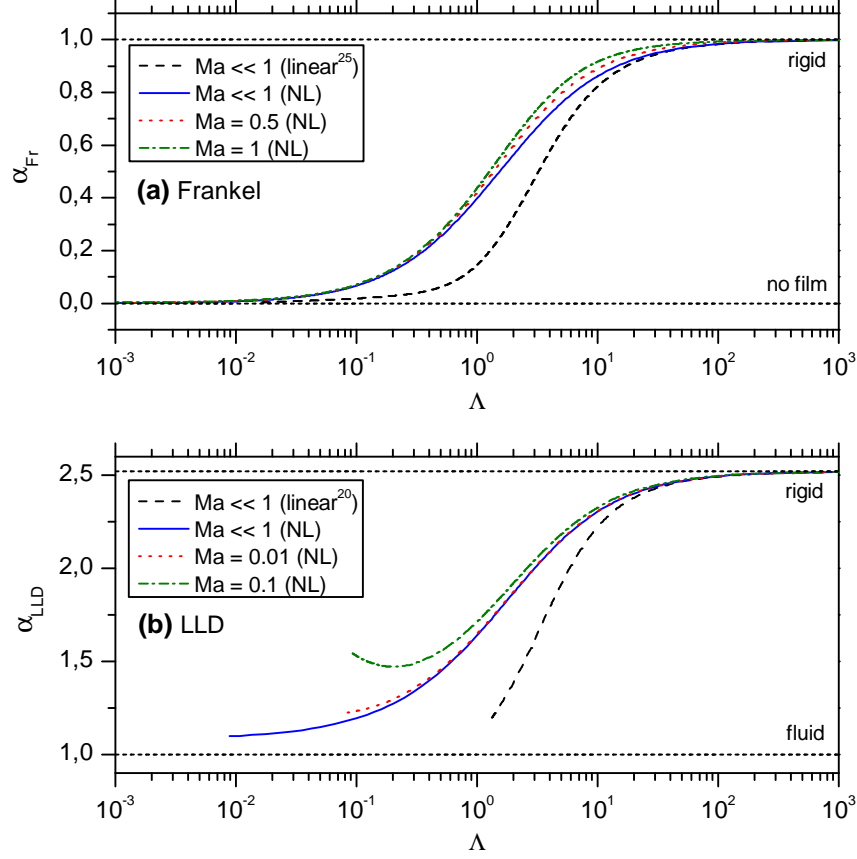


FIG. 8. The thickening factor α is plotted as a function of the dimensionless parameter Λ for (a) Frankel configuration and (b) LLD configuration. The different curves were obtained under different assumptions: *non-linear* equation of state and $\text{Ma} \ll 1$ (solid lines), *linear* equation of state and $\text{Ma} \ll 1$ (long-dashed lines), non-linear equation of state and finite values for Ma (dotted and dot-dashed lines). Note that, for a typical Marangoni number $\text{Ma} \sim 10^{-2}$ (as obtained from the experimental data) and capillary numbers between 10^{-6} and 10^{-3} , the control parameter Λ ranges from 1 to 10^2 .

state (14) instead of using its linearized version:

$$\gamma(\Gamma) = \gamma_0 - E \frac{\Gamma - \Gamma_0}{\Gamma_0}. \quad (\text{A1})$$

The main consequence of this choice is that the surface tension gradient writes $\partial_x \gamma = -E \Gamma' / \Gamma$ in our case, instead of $\partial_x \gamma = -E \Gamma' / \Gamma_0$ in the linear case. Using the conservation of surfactants at the interface eq. (22), the surface tension gradient can be expressed independently of the surface concentration as $\partial_x \gamma = E u_s' u_s / u_s^2$ in the non-linear case and $\partial_x \gamma = E u_s^* u_s' / u_s^2$ in the linear case, where the surface velocity u_s^* at the junction between the dynamic and static menisci remains to be determined.

Still under the assumption $Ma \ll 1$ in equations (21) and (26), which shall be precised in the last paragraph of this section, we compute the thickening factor α_{Fr} (resp. α_{LLD}) in Frankel configuration (resp. in LLD configuration) defined as

$$\alpha_{\text{Fr}} = \frac{h''(-\infty)}{\sqrt{2} K_{\text{Fr}}} \quad \left(\text{resp.} \quad \alpha_{\text{LLD}} = \frac{h''(-\infty)}{\sqrt{2} K_{\text{LLD}}^{\text{fluid}}} \right), \quad (\text{A2})$$

as a function of the control parameter Λ . Comparison to equation (28) shows that the thickening factor α_{Fr} (resp. α_{LLD}) is simply the ratio between the film thickness predicted by our model and the one predicted by the Frankel (resp. LLD) model.

The function $\alpha_{\text{Fr}}(\Lambda)$ (resp. $\alpha_{\text{LLD}}(\Lambda)$) is computed using the *linearized* equation of state eq. (A1) (dashed line) and compared to our solution with the non-linear equation of state (solid line) in figure 8a (resp. 8b). Note the dashed line in figure 8a (resp. 8b) had previously been obtained by ref.⁵ (resp. ref.²⁷) for soap film pulling and plate coating respectively. For both configurations, we observe the following discrepancies between the results obtained with the linear and non-linear equations of state:

- i) The linearized equation of state gives a sharper transition between the rigid and fluid behaviors: the transitions only spans over two decades, instead of three for the non-linearized equation of state,
- ii) Using the linearized equation of state can lead to significant underestimation of the film thickness (up to a factor of 3 for $\Lambda \sim 1$ in the case of soap films), and thus on the deduced surface elasticity, in the range of Λ probed experimentally ($\Lambda = 10^{-1} - 10^2$),
- iii) In Frankel configuration, the curve $h_0(\text{Ca})$ reconstructed using the linearized equation of state (*i.e.* from the dashed line in figure 8a) goes through a maximum, as shown in reference⁵. On the contrary, the reconstruction using the non-linear equation of state (*i.e.* from the solid line in figure 8a) yields a monotonous increase of the thickness with Ca .

For Frankel configuration, the fully rigid case (Frankel's model) is recovered at large Λ , namely at large Marangoni number or low capillary number, no matter the equation of state. For low Λ , the thickness tends to zero: in practice, the interfacial stresses are no longer sufficient to pull a stable film, hence the “no film” limit in figure 8a (lower short-dashed line).

For LLD configuration, the maximal thickening factor $4^{2/3} \approx 2.52$ corresponding to the fully rigid case is also obtained at large Λ for both the linear and non-linear equation of state. However, the fluid limit $\alpha_{\text{LLD}} = 1$ of the LLD model is not recovered for small values of Λ , neither for the linearized nor for the non-linearized equation of state. This is likely due to a loss of convergence in our numerical calculations when decreasing Λ , and is associated with the impossibility for the surface concentration to be negative, physically, and mathematically, as inferred from eq. (14). As illustrated in figure 9 for LLD configuration, the concentration in the flat film $\Gamma(0)$ tends to zero when decreasing Λ , and so does the surface velocity in the static meniscus $u_s(-\infty)$, since they are related by the conservation law eq. (18). A similar curve is obtained for the Frankel configuration and the conclusions are identical (data not shown). This is the reason why the curves in figure 8 are stopped when no convergence is obtained. Note that the position of the stopping point is very sensitive to the model used and that our simplified model (solid curves) provides the widest range of converged solutions.

The Marangoni term in equations (21), (24) (subsection IIIB) and (26) (subsection IIIC) has been neglected under the assumption $Ma \ll 1$. Figure 8 compares the curves $\alpha_{\text{Fr}}(\Lambda)$ and $\alpha_{\text{LLD}}(\Lambda)$

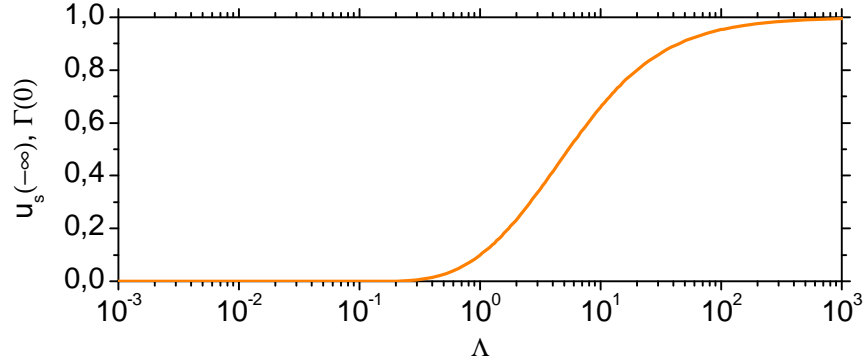


FIG. 9. The surface velocity in the static meniscus $u_s(-\infty)$ is plotted as a function of the control parameter Λ . Note that $u_s(-\infty)$ is equal to the surface concentration in the flat part of the film $\Gamma(0)$ thanks to the surfactant number conservation eq. (18).

obtained by solving the system including the Marangoni terms (dotted and dot-dashed lines) to the ones obtained by solving the approximated system (solid lines). All predictions including the Marangoni terms fall on top of the approximated solution for $\text{Ma} \lesssim 0.1$ in the case of soap films (data not shown) and for $\text{Ma} \lesssim 0.01$ in the case of coated films (data not shown). Consequently, the assumption $\text{Ma} \ll 1$ does not have the same meaning in Frankel and LLD configurations, but remains valid in both cases given the values of Ma extracted from the fit of the experimental data (see table I).

Appendix B: Non-linear fit of h_0 vs Ca

1. Frankel configuration

For practical use, we here propose a non-linear fit of the thickening factor α_{Fr} defined as h_0 divided by the half film thickness predicted by Frankel's model, namely $K_{\text{Fr}} \ell_c \text{Ca}^{2/3}$:

$$\alpha_{\text{Fr}}(\Lambda) \approx \frac{1}{2} \left[1 + \tanh(186.3 - 186.1 \Lambda^{0.0026}) \right]. \quad (\text{B1})$$

The theoretical half film thickness as a function of the capillary number is then recovered for a given Marangoni number through

$$h_0(\text{Ca}) = K_{\text{Fr}} \ell_c \text{Ca}^{2/3} \times \alpha_{\text{Fr}} \left(\frac{\text{Ma}}{\text{Ca}^{2/3}} \right). \quad (\text{B2})$$

2. LLD configuration

Similarly, we propose a non-linear fit of the thickening factor α_{LLD} defined as h_0 divided by the half film thickness predicted by LLD model in the fluid limit, namely $K_{\text{LLD}}^{\text{fluid}} \ell_c \text{Ca}^{2/3}$:

$$\alpha_{\text{LLD}}(\Lambda) \approx \frac{1}{2} \left[3.603 - 1.436 \tanh(15.75 - 15.52 \Lambda^{0.030}) \right]. \quad (\text{B3})$$

Since $K_{\text{LLD}}^{\text{fluid}} = K_{\text{Fr}}$, the theoretical film thickness as a function of the capillary number is also obtained from eq. (B2), replacing the function α_{Frankel} by α_{LLD} for coated films.

ACKNOWLEDGMENTS

The authors would like to thank Dominique Langevin for valuable advice and comments. L.C. was supported by ANR F2F. B.S. thanks the F.R.S.-FNRS for funding as well as the IAP-MicroMAST project for supporting this research. This work was performed under the umbrella of COST Action MP1106.

- ¹P. Stevenson, *Foam engineering: fundamentals and applications* (Wiley.com, 2012).
- ²B. Bhushan and B. K. Gupta, *Handbook of tribology: materials, coatings, and surface treatments* (McGraw-Hill, New York, NY (United States), 1991).
- ³S. F. Kistler and P. M. Schweizer, *Liquid film coating* (Springer, 1997).
- ⁴E. A. Van Nierop, B. Scheid, and H. A. Stone, “On the thickness of soap films: an alternative to frankel’s law–corrigendum,” *Journal of fluid mechanics* **630**, 443–443 (2009).
- ⁵J. Seiwert, B. Dollet, and I. Cantat, “Theoretical study of the generation of soap films: role of interfacial viscoelasticity,” *Journal of Fluid Mechanics* **739**, 124–142 (2014).
- ⁶K. J. Mysels, S. Frankel, and K. Shinoda, *Soap films: studies of their thinning and a bibliography* (Pergamon Press, 1959).
- ⁷R. Bruinsma, J. M. Di Meglio, D. Quéré, and S. Cohen-Addad, “Formation of soap films from polymer solutions,” *Langmuir* **8**, 3161–3167 (1992).
- ⁸B. Scheid, E. A. van Nierop, and H. A. Stone, “Thermocapillary-assisted pulling of thin films: Application to molten metals,” *Applied physics letters* **97**, 171906–171906 (2010).
- ⁹B. Scheid, E. A. van Nierop, and H. A. Stone, “Thermocapillary-assisted pulling of contact-free liquid films,” *Physics of fluids* **24**, 032107 (2012).
- ¹⁰L. Landau and B. Levich, “Dragging of a liquid by a moving plate,” *Acta Physicochim. USSR*. **17**, 42–54 (1942).
- ¹¹J. Snoeijer, J. Ziegler, B. Andreotti, M. Fermigier, and J. Eggers, “Thick films of viscous fluid coating a plate withdrawn from a liquid reservoir,” *Physical Review Letters* **100**, 244502 (2008).
- ¹²J. Delacotte, L. Montel, F. Restagno, B. Scheid, B. Dollet, H. A. Stone, D. Langevin, and E. Rio, “Plate coating: Influence of concentrated surfactants on the film thickness,” *Langmuir* **28**, 3821–3830 (2012).
- ¹³L. M. Sagis, “Dynamic properties of interfaces in soft matter: Experiments and theory,” *Reviews of Modern Physics* **83**, 1367 (2011).
- ¹⁴S. Lioni-Addad and J. M. di Meglio, “Stabilization of aqueous foam by hydrosoluble polymers. 1. sodium dodecyl sulfate-poly (ethylene oxide) system,” *Langmuir* **8**, 324–327 (1992).
- ¹⁵J. Lal and J.-M. di Meglio, “Formation of soap films from insoluble surfactants,” *Journal of colloid and interface science* **164**, 506–509 (1994).
- ¹⁶E. A. Adelizzi and S. M. Troian, “Interfacial slip in entrained soap films containing associating hydrosoluble polymer,” *Langmuir* **20**, 7482–7492 (2004).
- ¹⁷S. Berg, E. A. Adelizzi, and S. M. Troian, “Experimental study of entrainment and drainage flows in microscale soap films,” *Langmuir* **21**, 3867–3876 (2005).
- ¹⁸L. Saulnier, F. Restagno, J. Delacotte, D. Langevin, and E. Rio, “What is the mechanism of soap film entrainment?” *Langmuir* **27**, 13406–13409 (2011).
- ¹⁹F. C. Morey, “Thickness of a liquid film adhering to surface slowly withdrawn from the liquid,” *J. Res. Nat. Bur. Stand.* **25**, 385–393 (1940).

- ²⁰R. Homsy and G. M. Krechetnikov, “Experimental study of substrate roughness and surfactant effects on the landau-levich law,” *Physics of Fluids* **17**, 102108 (2005).
- ²¹D. Qu  r  , “Fluid coating on a fiber,” *Annual Review of Fluid Mechanics* **31**, 347–384 (1999).
- ²²A. Q. Shen, B. Gleason, G. H. McKinley, and H. A. Stone, “Fiber coating with surfactant solutions,” *Physics of Fluids* **14**, 4055–4068 (2002).
- ²³F. Bretherton, “The motion of long bubbles in tubes,” *J. Fluid Mech* **10**, 166–188 (1961).
- ²⁴E. A. Van Nierop, B. Scheid, and H. A. Stone, “On the thickness of soap films: an alternative to frankel’s law,” *Journal of fluid mechanics* **602**, 119 (2008).
- ²⁵E. van Nierop, D. Keupp, and H. Stone, “Formation of free films of aqueous solutions of poly-(ethylene oxide): The influence of surfactant,” *Europhysics Letters* **88**, 66005 (2009).
- ²⁶D. A. White and J. A. Tallmadge, “Theory of drag out of liquids on flat plates,” *Chemical Engineering Science* **20**, 33–37 (1965).
- ²⁷C.-W. Park, “Effects of insoluble surfactants on dip coating,” *Journal of colloid and interface science* **146**, 382–394 (1991).
- ²⁸K. J. Stebe, S.-Y. Lin, and C. Maldarelli, “Remobilizing surfactant retarded fluid particle interfaces. i. stress-free conditions at the interfaces of micellar solutions of surfactants with fast sorption kinetics,” *Physics of Fluids* **3**, 3–20 (1991).
- ²⁹L. Schwartz and R. Roy, “Modeling draining flow in mobile and immobile soap films,” *Journal of colloid and interface science* **218**, 309–323 (1999).
- ³⁰N. Tiwari and J. M. Davis, “Theoretical analysis of the effect of insoluble surfactant on the dip coating of chemically micropatterned surfaces,” *Physics of Fluids* **18**, 022102 (2006).
- ³¹D. M. Campana, “Numerical prediction of the film thickening due to surfactants in the landau-levich problem,” *Journal of colloid interface science* **22**, 032103 (2010).
- ³²J. Lucassen, “Dynamic properties of free liquid films and foams,” *Anionic surfactants: physical chemistry of surfactant action* **11**, 217–265 (1981).
- ³³A. Sonin, A. Bonfillon, and D. Langevin, “Thinning of soap films: The role of surface viscoelasticity,” *Journal of colloid and interface science* **162**, 323–330 (1994).
- ³⁴B. Scheid, J. Delacotte, B. Dollet, E. Rio, F. Restagno, E. Van Nierop, I. Cantat, D. Langevin, and H. A. Stone, “The role of surface rheology in liquid film formation,” *Europhysics Letters* **90**, 24002 (2010).
- ³⁵A. Prins, C. Arcuri, and M. Van Den Tempel, “Elasticity of thin liquid films,” *Journal of Colloid and Interface Science* **24**, 84–90 (1967).
- ³⁶E. Lucassen-Reynders, A. Cagna, and J. Lucassen, “Gibbs elasticity, surface dilational modulus and diffusional relaxation in nonionic surfactant monolayers,” *Colloids and Surfaces A* **186**, 63–72 (2001).
- ³⁷L. Saulnier, Ph.D. thesis, Universit   Paris-Sud (2012).
- ³⁸E. Doedel, R. Paffenroth, A. Champneys, T. Fairgrieve, Y. A. Kuznetsov, B. Oldeman, B. Sandstede, and X. Wang, “Auto-07p: Continuation and bifurcation software for ordinary differential equations,” (2007), available for download from <http://indy.cs.concordia.ca/auto>.
- ³⁹R. L. Bendure, “Dynamic surface tension determination with the maximum bubble pressure method,” *Journal of Colloid and Interface Science* **35**, 238–248 (1971).
- ⁴⁰S.-Y. Lin, Y.-C. Lee, and M.-J. Shao, “Adsorption kinetics of c12e6 at the air-water interface,” *Journal of the Chinese Institute of Chemical Engineers* **33**, 631–643 (2002).
- ⁴¹H. Ritacco, D. Langevin, H. Diamant, and D. Andelman, “Dynamic surface tension of aqueous solutions of ionic surfactants: role of electrostatics,” *Langmuir* **27**, 1009–1014 (2011).
- ⁴²D. K. Owens, “The dynamic surface tension of sodium dodecyl sulfate solutions,” *Journal of Colloid and Interface Science* **29**, 496–501 (1969).
- ⁴³D. C. Henderson and F. J. Micale, “Dynamic surface tension measurement with the drop mass technique,” *Journal of colloid and interface science* **158**, 289–294 (1993).
- ⁴⁴C. Stenvot and D. Langevin, “Study of viscoelasticity of soluble monolayers using analysis of propagation of excited capillary waves,” *Langmuir* **4**, 1179–1183 (1988).
- ⁴⁵N. Adami and H. Caps, “Surface tension profiles in vertical soap films,” (2013), arXiv:1310.0454 [physics.flu-dyn].
- ⁴⁶L. Saulnier, L. Champougny, G. Bastien, F. Restagno, D. Langevin, and E. Rio, “A study of generation and rupture of soap films,” *Soft Matter* (2014).
- ⁴⁷O. Ou Ramdane and D. Qu  r  , “Thickening factor in marangoni coating,” *Langmuir* **13**, 2911–2916 (1997).